RESTRICTED

COPY NO. 105

RM No. E7B11d

NACA

RESEARCH MEMORANDUM

COOLING OF GAS TURBINES

IV - CALCULATED TEMPERATURE DISTRIBUTION IN THE TRAILING PART OF A TURBINE BLADE USING DIRECT LIQUID COOLING

By W. Byron Brown and William R. Monroe

Aircraft Engine Research Laboratory
Cleveland, Ohio

CLASSIFIED DOCUMENT

This document contains classified information affecting the National Defense of the United States within the meaning of the Espionage Act, USC 50:31 and 32. Its transmission or the revelation of its contents in any manner to an unauthorized person is prohibited by law. Information so classified may be imparted only to persons in the military and naval Services of the United States, appropriate civilian officers and employees of the Federal Government who have a legitimate interest therein, and to United States citizens of known loyalty and discretion who of necessity must be informed thereof.

TECHNICAL EDITING WAIVED

NATIONAL ADVISORY COMMITTEE FOR AERONAUTICS

WASHINGTON

April 18, 1947

RESTRICTED

NATIONAL ADVISORY COMMITTEE FOR AERONAUTICS

RESEARCH MEMORANDUM

COOLING OF GAS TURBINES

IV - CALCULATED TEMPERATURE DISTRIBUTION IN THE TRAILING PART OF A TURBINE BLADE USING DIRECT LIQUID COOLING

By W. Byron Brown and William R. Monroe

SUMMARY

A theoretical analysis was made to determine the temperature distribution in the trailing portion of a liquid-cooled turbine blade between the coolant passage and the trailing edge and to study the influence of various design and operating variables on the hot-spot temperature at the trailing edge. The trailing portion of a typical turbine blade was approximated by equivalent rectangular and wedge-shaped sections to facilitate analysis, and representative values for the boundary temperatures and surface heat-transfer coefficients were assumed or computed according to standard methods.

Three-dimensional temperature distributions were obtained at effective gas temperatures of 2000°, 3000°, and 5000° F for a 4-inch prismatic section, cooled over the entire length and having a thermal conductivity of 15 Btu per hour per foot per °F, and at 2000° F for similar sections having thermal conductivities of 120 and 210 Btu per hour per foot per °F. In addition, comparison of one-dimensional temperature distributions through the outer portion of the blade was made for two shapes, equivalent rectangular and wedge plane sections, at an effective gas temperature of 2000° F. The influence of thermal conductivity on one-dimensional temperature distribution in both plane sections was evaluated. With the equivalent rectangular solution, an investigation was made to determine the effect on trailing-edge hot-spot temperature of variations in the trailing-section width, thickness, thermal conductivity, and coolant-passage heat-transfer coefficient.

The three-dimensional and one-dimensional solutions of the equivalent rectangular trailing portion give almost identical temperature distribution in the blade section away from the influence of

rim cooling. For the blades of low thermal conductivity and wide trailing sections the hot-spot temperature closely approaches the effective gas temperature, and infinite increase in the surface heat-transfer coefficient at the coolant passage relative to that obtained with water will have small effect on the trailing-edge temperature. Further reduction of trailing-edge hot-spot temperature can be obtained by the following three methods given in order of decreasing effect; by use of materials having high thermal conductivity, by altering the blade shape to provide a relatively short trailing portion, by locating additional cooling passages a short distance from the trailing edge.

INTRODUCTION

As part of the general program to increase the permissible operating temperature of gas-turbine cycles and to improve the life of critical parts, further analysis of the liquid-cooled turbine blade is being conducted by the NACA to determine the available cooling effect at the anticipated hot spot under present conditions of design and to evaluate various possible methods of improving cooling of the blades.

Part I of the current series on "Cooling of Gas Turbines" (reference 1) presents calculations on the application of air cooling fins to the turbine rotor with the object of reducing the rim temperature to permit better cooling of solid blades. It was found that the root of the blade could be cooled about 800° F below the effective gas temperature, but relatively little gain was obtained at the critical section some distance from the root. In part II (reference 2) it was shown that blade life could be extended by rim cooling, and that the effective gas temperature could be slightly increased.

Part III (reference 3) discusses the circulation of liquids through hollow passages in the blade and presents a one-dimensional analysis of temperature distribution from the blade tip to the rotor axis. The effects of variations in blade length, length of cooling passage, type of liquid coolant, and rate of coolant flow were studied. The temperatures calculated (one-fifth the gas temperature for water cooling) were those appropriate to points near the cooling passages.

The purpose of the present detailed study is to investigate the temperature distribution encountered in the relatively long, thin trailing section between the coolant passage and the trailing edge

of the liquid-cooled blade. This section, particularly the trailing edge, seems most likely to be critical. The blade design and cooling conditions used are the same as used in reference 3 except that only the blade section bounded by the rim, the tip, the wall of the coolant passage, and the trailing edge is considered. The analysis is carried out in several parts, with assumed shapes or sections that approximate the trailing portion of a typical blade as follows: a one-dimensional analysis of a rectangular section through the outer portion away from the root, a similar one-dimensional analysis of a wedge-shaped section, and a three-dimensional analysis of a right prism for the entire span of the blade.

The following sections of this report present the development of the various solutions for temperature distribution in terms of the dimensions, physical properties, boundary temperatures, and surface conditions that prevail. In addition, a number of figures are presented that illustrate the various effects of thermal conductivity on three-dimensional temperature distribution for several values of the effective gas temperature and the combined influence of design dimensions, thermal conductivity, and some surface conditions on cooling of the trailing edge.

THEORETICAL ANALYSIS

Symbols

The following symbols, arranged in alphabetical order for the convenience of the reader, were used in the calculations:

a parameter equal to $\sqrt{\frac{2q_i}{kt}}$, (ft^{-1})

b distance from trailing edge to wall of coolant passage, (ft)

k thermal conductivity of turbine metal, Btu/(hr)(ft)($^{\circ}$F)

l distance from blade tip to rim, (ft)

q_i heat-transfer coefficient from hot gas to metal, Btu/(hr)(sq ft)($^{\circ}$F)

q_o heat-transfer coefficient from metal to coolant, Btu/(hr)(sq ft)($^{\circ}$F)

t blade thickness, (ft)

$\bar{t}$ mean blade thickness, (ft)

t_1 blade thickness at trailing edge, (ft)

t_2 blade thickness at wall of coolant passage, (ft)

T temperature of metal, $^{\circ}F$

T_e effective temperature of hot gas, $^{\circ}F$

T_l average temperature of liquid coolant, $^{\circ}F$

T_r temperature at rim, $^{\circ}F$

x distance from blade tip to blade element, (ft)

y distance from trailing edge to blade element, (ft)

z distance from median plane of section to blade element, (ft)

2α angle between sloping sides of wedge

θ $T_e - T$, $^{\circ}F$

A linear dimension accented by a prime denotes that the distance has been extended by $t_1/2$ (for the wedge) or $\bar{t}/2$ (for the rectangle).

Discussion of Simplifying Assumptions

The turbine wheel with cooling passages is shown in figure 1 and a cross section of the blade in figure 2. The approximate blade shapes (right prism, wedge, and rectangle) used in this analysis, which can be used to approximate any tapered profile, are given in figures 3, 4, and 5.

The equations for the temperature distribution in the blade section between the coolant passage and the trailing edge were obtained by equating the heat entering and the heat leaving an element. In order to simplify the boundary conditions, the cross section of the blade under consideration was approximated by geometric figures having straight sides and areas equal to that of the blade cross section. For the first development, a rectangular shape (fig. 3) was used, in which the width was made equal to the distance from the trailing edge to the coolant-passage wall and the thickness equal to the mean thickness of the blade over this width. For a

closer approximation to the true shape, a wedge shape (fig. 4) was used in which the width remained the same as in the rectangle and the thickness tapered from the blade thickness at the coolant passage to the blade thickness at the trailing edge. For both shapes, the approximate cooling surface was less than that encountered in the actual blade because the circular coolant-passage wall was approximated by a chord rather than by the true arc.

The analysis was performed in the following parts: (a) a one-dimensional analysis of a rectangular section through the outer portion of the blade, away from the blade root; (b) a one-dimensional analysis of a wedge-shaped section through the outer portion of the blade; and (c) a three-dimensional analysis of a right prism for a 4-inch blade length.

The following simplifying assumptions were made for these parts:

(1) In parts (a) and (b), the heat flow to the rim was negligible at a section chosen away from the blade root because the length l was large compared to the width b (fig. 5). The validity of this assumption is demonstrated by the results obtained in the three-dimensional analysis.

(2) The heat gained from the trailing edge can be accounted for by assuming the width to be extended by a distance equal to one-half the blade thickness at the trailing edge t_1 (fig. 6). The edge OQ at temperature T gained some heat. The extended surfaces OO' and QQ' were at nearly the same temperature T and no heat entered the end $O'Q'$, therefore these surfaces gained practically the same amount of heat as the actual exposed end. In part (c) especially, the boundary condition was much simplified. This assumption remained valid as long as $t/2$ was small compared with b. This validity is demonstrated for part (a). In like manner, the blade length was extended a distance equal to $t/2$. The length and the width extended by the distance $t/2$ are denoted by b' and l', respectively. This assumption was used only in parts (b) and (c).

(3) The temperature of the blade at the rim was constant at rim temperature. If this constancy is not maintained, it is shown that variations from it have little effect on the results except very close to the rim. This assumption was used only in part (c).

(4) The variation of k was negligible and T_e, T_l, q_i, and q_o are constant over the blade and surface passages. Because these blades were assumed to be cooled over the entire length and those of reference 3 cooled only to within one-sixteenth inch of the tip, the comparable curves differed at the tip.

The analysis of parts (a), (b), and (c) are given in the following sections.

One-Dimensional Analysis of Rectangular Section through Outer Portion of Blade, Away from Blade Root

The derivation of the formula for part (a) as shown by figure 3 is obtained from:

Heat entering element from right end = $kt\ d\theta/dy$

Heat entering element from sides = $2q_i\ dy\ \theta$

Heat leaving element from left end = $kt\ (d\theta/dy + d^2\theta/dy^2\ dy)$

Therefore,

$$kt\ d\theta/dy + 2q_i\ dy\ \theta = kt\ (d\theta/dy + d^2\theta/dy^2\ dy) \tag{1}$$

or

$$\frac{d^2\theta}{dy^2} = a^2\theta \tag{2}$$

where

$$a = \sqrt{\frac{2q_i}{kt}} \tag{3}$$

The boundary conditions are as follows:
when $y = b$,

$$kt\ \frac{d\theta}{dy} = q_o t\ (T - T_l)$$

If $T_e - \theta$ is substituted for T,

$$\frac{kd\theta}{dy} = q_o\ (T_e - T_l - \theta) \tag{4}$$

when $y = 0$,

$$k\ \frac{d\theta}{dy} = q_i\theta \tag{5}$$

A solution of equation (2) is

$$\theta = A \cosh a\ (y + \epsilon) \tag{6}$$

where A and ϵ are integration constants. The quantities ϵ and A are evaluated to satisfy the boundary conditions at the blade edge and in the cooling passage, respectively.

From equations (5) and (6), when $y = 0$,

$$kA\, a \sinh a\, \epsilon = q_i\, A \cosh a\, \epsilon \tag{7}$$

therefore from equations (3) and (7)

$$\epsilon = \frac{\tanh^{-1}\left(\frac{q_i}{ka}\right)}{a} = \frac{\tanh^{-1} a\left(\frac{t}{2}\right)}{a} \approx \frac{t}{2} \tag{8}$$

when t is not too large. This difference between ϵ and $t/2$ varies from 0.4 to 0.5 percent for the values of a considered and has an inappreciable effect 0.005 foot or more inside the trailing edge.

When $y = b$, then from equations (4) and (6)

$$Aa \sinh a\,(b + \epsilon) = \frac{q_o}{k}\left[T_e - T_l - A \cosh a\,(b + \epsilon)\right] \tag{9}$$

or

$$A = \frac{\frac{q_o}{k}(T_e - T_l)}{a \sinh a\,(b + \epsilon) + \frac{q_o}{k} \cosh a\,(b + \epsilon)} \tag{10}$$

Therefore,

$$\theta = \frac{\frac{q_o}{k}(T_e - T_l) \cosh a\,(y + \epsilon)}{a \sinh a\,(b + \epsilon) + \frac{q_o}{k} \cosh a\,(b + \epsilon)} \tag{11}$$

One-Dimensional Analysis of Wedge-Shaped Section through Outer Portion of Blade

It has been demonstrated (reference 4, equation (53)) that a solution for the temperature distribution along the y-axis in a wedge-shaped segment (fig. 4) may be expressed

$$\theta = A' J_o(i\mu) + B i H_o(i\mu) \tag{12}$$

where A' and B are arbitrary constants and J_o and H_o are Bessel's functions of two kinds, zero order.

The variable μ is defined

$$\mu^2 = 4C^2 \left[y' + t_1 \left(\frac{1 - \tan \alpha}{2 \tan \alpha} \right) \right] \tag{13}$$

where

$$C^2 = \frac{q_i}{k \sin \alpha} \tag{14}$$

and

$$\alpha = \tan^{-1} \left(\frac{t_2 - t_1}{2b} \right) \tag{15}$$

The boundary conditions are, when $y' = 0$

$$\frac{d\theta}{dy'} = 0 \tag{16}$$

when $y' = b'$

$$k \frac{d\theta}{dy'} = q_o \left(T_e - T_l - \theta \right) \tag{17}$$

or when $\mu = \mu_1$

$$\frac{d\theta}{d\mu} = 0$$

and when $\mu = \mu_2$

$$k \frac{2C^2}{\mu_2} \frac{d\theta}{d\mu} = q_o \left(T_e - T_l - \theta \right)$$

when $y' = 0$

$$\mu_1 = 2C \sqrt{\frac{t_1 \left(1 - \tan \alpha \right)}{2 \tan \alpha}} \tag{18}$$

when $y' = b'$

$$\mu_2 = 2C \sqrt{b' + t_1 \left(\frac{1 - \tan \alpha}{2 \tan \alpha} \right)} \tag{19}$$

Equation (13) can be differentiated and put in the form $\frac{d\theta}{d\mu}$, giving

$$\frac{d\theta}{d\mu} = \frac{\mu}{2C^2} \frac{d\theta}{dy'} \tag{20}$$

Therefore when

$$\frac{d\theta}{dy'} = 0$$

then

$$\frac{d\theta}{d\mu} = 0 \tag{21}$$

By virtue of the properties of Bessel's functions,

$$dJ_o (y)/dy = -J_1 (y)$$

and

$$dH_o(y)/dy = -H_1(y)$$

therefore

$$\frac{d\theta}{d\mu} = -A'iJ_1(i\mu) + B\,H_1(i\mu) \tag{22}$$

and when

$$\frac{d\theta}{d\mu} = 0$$

then

$$B = \frac{iA'J_1(i\mu_1)}{H_1(i\mu_1)} \tag{23}$$

In order that equation (17) may be satisfied

$$k\frac{2C^2}{\mu_2}[-A'i\,J_1(i\mu_2) + BH_1(i\mu_2)] = q_o[(T_e-T_l) - A'J_o(i\mu_2) - Bi\,H_o(i\mu_2)] \tag{24}$$

In standard form equations (23) and (24) can be written, respectively

$$[iJ_1(i\mu_1)]\,A' - [H_1(i\mu_1)]\,B = 0$$

$$\left[J_o(i\mu_2) - \frac{2C^2k}{q_o\mu_2}iJ_1(i\mu_2)\right]A' + \left[\frac{2C^2k}{q_o\mu_2}H_1(i\mu_2) + iH_o(i\mu_2)\right]B = T_e - T_l$$

The values of A' and B can easily be found and substituted into equation (12), giving θ in the form

$$\theta = \frac{\frac{q_o\mu_2}{2C^2k}(T_e-T_l)\,[H_1(i\mu_1)J_o(i\mu) + iJ_1(i\mu_1)iH_o(i\mu)]}{[iJ_1(i\mu_1)H_1(i\mu_2)] - [H_1(i\mu_1)iJ_1(i\mu_2)] + \frac{q_o\mu_2}{2C^2k}X} \tag{25}$$

where X is

$$[H_1(i\mu_1)J_o(i\mu_2) + iJ_1(i\mu_1)iH_o(i\mu_2)]$$

Three-Dimensional Analysis of Right Prism for 4-Inch Blade Length

The derivation of the formula for part (c) as shown in figure 5 is obtained from

Heat entering element from top = $-k\ dydz\ \frac{\partial T}{\partial x}$

Heat entering element from right end = $-k\ dxdz\ \frac{\partial T}{\partial y}$

Heat entering element from front = $-k\ dxdy\ \frac{\partial T}{\partial z}$

Heat leaving element from bottom = $-k\ dydz\left(\frac{\partial T}{\partial x} + \frac{\partial^2 T}{\partial x^2}\,dx\right)$

Heat leaving element from left end = $-k\ dxdz\left(\frac{\partial T}{\partial y} + \frac{\partial^2 T}{\partial y^2}\,dy\right)$

Heat leaving element from back = $-k\ dxdy\left(\frac{\partial T}{\partial z} + \frac{\partial^2 T}{\partial z^2}\,dz\right)$

When the heat entering is equated to the heat leaving

$$-k\ dydz\ \frac{\partial T}{\partial x} - k\ dxdz\ \frac{\partial T}{\partial y} - k\ dxdy\ \frac{\partial T}{\partial z} = -k\ dydz\left(\frac{\partial T}{\partial x} + \frac{\partial^2 T}{\partial x^2}\,dx\right) - k\ dxdz\left(\frac{\partial T}{\partial y} + \frac{\partial^2 T}{\partial y^2}\,dy\right) - k\ dxdy\left(\frac{\partial T}{\partial z} + \frac{\partial^2 T}{\partial z^2}\,dz\right) \tag{26}$$

or

$$0 = \frac{\partial^2 T}{\partial x^2} + \frac{\partial^2 T}{\partial y^2} + \frac{\partial^2 T}{\partial z^2} \tag{27}$$

The boundary conditions can be more simply handled if the gas temperature is taken as a reference temperature rather than the metal temperature; that is, if the substitution is made

$$\theta = T_e - T \tag{28}$$

or

$$T = T_e - \theta \tag{29}$$

Equation (27) then becomes

$$0 = \frac{\partial^2 \theta}{\partial x'^2} + \frac{\partial^2 \theta}{\partial y'^2} + \frac{\partial^2 \theta}{\partial z^2} \tag{30}$$

The origin of the coordinates chosen is indicated in figure 5. The axis $z = 0$ is located in the median plane of the right prism; from considerations of symmetry there can be no heat flow across the median plane.

The boundary conditions that must be satisfied are

when $x' = 0$

$$\frac{\partial\theta}{\partial x'} = 0 \tag{31}$$

when $y' = 0$

$$\frac{\partial\theta}{dy'} = 0 \tag{32}$$

when $z = 0$

$$\frac{\partial\theta}{\partial z} = 0 \tag{33}$$

when $x' = l'$

$$\theta = T_e - T_r \tag{34}$$

when $y' = b'$

$$\frac{k\partial\theta}{\partial y'} = q_o\,(T_e - T_l - \theta) \tag{35}$$

when $z = \frac{t}{2}$

$$\frac{k\partial\theta}{\partial z} = -q_i\,\theta \tag{36}$$

A convenient form for the solution of equation (30) is

$$\theta = \sum_{1}^{\infty}{}_m \sum_{1}^{\infty}{}_n \times (A_{mn} \cos N_n x' \cosh M_{mn} y' \cos P_m z + B_{mn} \cosh R_{mn} x' \cos \lambda_n y' \cos P_m z) \tag{37}$$

where A, B, M, N, R, λ, and P are arbitrary constants. The relation between the constants used as coefficients for the variables is

$$M_{mn}^2 = P_m^2 + N_n^2 \tag{38}$$

$$R_{mn}^2 = P_m^2 + \lambda_n^2 \tag{39}$$

where $n = 1, 2, 3, 4, \ldots$, and $m = 1, 2, 3, 4, \ldots$. By the selection of equation (37), the boundary conditions expressed in equations (31) to (33) are satisfied.

In appendix A, values of A_{mn} and B_{mn} are derived. These values are

$$A_{mn} = \frac{(-1)^{n-1}}{\pi(2n-1)} \frac{\sin \frac{P_m t}{2}}{P_m \frac{t}{2}} \frac{8q_o (T_e - T_1)}{1 + \frac{\sin 2P_m \frac{t}{2}}{2P_m \frac{t}{2}}} \frac{1}{kM_{mn} \sinh M_{mn}b' + q_o \cosh M_{mn}b'}$$

$$B_{mn} = \frac{\sin \lambda_n b'}{\lambda_n b'} \frac{4 (T_e - T_r)}{1 + \frac{\sin 2\lambda_n b'}{2\lambda_n b'}} \frac{\sin P_m \frac{t}{2}}{P_m \frac{t}{2}} \frac{1}{1 + \frac{\sin 2P_m \frac{t}{2}}{2P_m \frac{t}{2}}} \frac{1}{\cosh R_{mn} l'}$$

Values of n from 1 to 14 were inserted and the temperatures calculated from equation (37).

In appendix B it is shown that sufficiently accurate results (within 1°) can be obtained by using only the first value of m; that is, $m = 1$ and dropping the terms involving $\cos P_2 z$, $\cos P_3 z$, etc.

APPLICATION OF ANALYSIS

The following assumptions were made in applying the previous results to specific numerical calculations:

1. The gas flow was 55 pounds per second. The heat-transfer coefficient corresponding to this gas flow q_i was found to be 222 Btu per hour per square foot per °F.

2. The liquid coolant, water, had an average temperature of 200° F and a flow rate of 6.42 pounds per second for the entire rotor. The heat-transfer coefficient corresponding to this coolant flow q_o was calculated (reference 5) as 2370 Btu per hour per square foot per °F.

3. Average thermal conductivities k of 15, 40, 60, 80, 100, 120, and 210 Btu per hour per square foot per °F were used.

4. The turbine had 55 blades.

5. The blade was liquid cooled over its entire length of 4 inches by two cooling passages 0.25 inch in diameter. The blade chord was 1.188 inches long.

6. Some numerical values assumed were

b = 0.0500 foot

b' = 0.0550 foot (rectangular section)

b' = 0.0515 foot (wedge-shaped section)

l = 0.3333 foot

l' = 0.3383 foot

$\bar{t}$ = 0.010 foot (rectangular section)

t_1 = 0.003 foot (wedge-shaped section)

t_2 = 0.021 foot (wedge-shaped section)

T_r = 284° F (all values of thermal conductivity) when T_e = 2000° F

T_r = 331° F (all values of thermal conductivity) when T_e = 3000° F

T_r = 426° F (all values of thermal conductivity) when T_e = 5000° F

The theoretical temperature distribution in the trailing segment of the turbine blade was determined by a three-dimensional analysis using equation (62) in which the blade cross section was approximated by a rectangle. The temperature distribution was found in two planes representing the maximum and the minimum temperatures for the z axis; the first plane was located at the side of the rectangle and the second was on the median plane through the section. The temperature was plotted against radial distance from the wheel axis for intervals from the trailing edge to the wall of the coolant passage (fig. 7). At the wall, the series converges too slowly to be useful, therefore the curve was based on a one-dimensional calculation (equation (11)) and the behavior of the other curves of the family. Similar distributions were calculated and plotted using thermal conductivities 120 and 210 Btu per hour per foot per °F (fig. 8).

The next step in the analysis was to determine the effect of using a rectangular cross section as an approximation of the true blade shape. The complexity of a solution using the true blade cross section eliminates an exact comparison. A wedge-shaped cross section

represents the closest approximation with planes as boundaries and this shape was used to indicate the trend. A three-dimensional analysis of a wedge-shaped cross section was beyond the scope of this report and quite unnecessary because on the outer three-quarters of the blade, the metal temperature does not change with the radius and the comparison was made on a one-dimensional basis for temperatures along the center line of a section through the outer portion of the blade. The comparison is presented as a plot of metal temperature against distance from the wall of the coolant passage for an equivalent rectangular and wedge-shaped section (fig. 9).

The thermal conductivity of the metals used in blade construction has considerable influence on the temperature distribution; the high-tensile-strength alloys currently used have a relatively low thermal conductivity. The effect of thermal conductivity was investigated using a one-dimensional analysis of a section through the outer portion of the blade for average thermal conductivities ranging from 15 (steel) to 210 Btu per hour per foot per $^{\circ}$F (copper). Although the upper range of conductivities is impracticable for actual use in blade construction, it does indicate the trend and the magnitude of temperature changes with changes in thermal conductivity. The comparison is presented as plots of metal temperature against distance from the wall of the coolant passage for the rectangular shape (fig. 10(a)) and the wedge shape (fig. 10(b)). The effect of a change in thermal conductivity on trailing-edge temperature was determined comparatively using the same values of conductivity for equivalent rectangular and wedge shapes. One station on the section center line at the trailing edge was used for each thermal conductivity (fig. 11).

RESULTS AND DISCUSSION

The theoretical three-dimensional temperature distribution for a turbine blade of rectangular cross section is presented for effective gas temperatures of 2000°, 3000°, and 5000° F in figure 7. The temperature falls off in increasing increments as the distance to the cooling liquid decreases. At a constant distance from the wall of the coolant passage, the temperature remains substantially constant for approximately three-quarters of the blade length. The temperature beyond this point falls off rapidly and reaches the rim temperature at the base. The average temperature at the trailing edge of the blade was reduced 7.14 percent below the gas temperature at 2000° F and 7.6 percent below the gas temperature at 5000°. The temperature differential between the side and the center of the blade ($z = t/2$) was 3.6 percent of θ, negligible at the trailing edge, and at the maximum point did not exceed 5 percent of the metal temperature.

The temperature distribution at a gas temperature of 2000° F for rectangular blades having thermal conductivities of 120 and 210 Btu per hour per foot per °F is presented in figure 8. With increasing thermal conductivity of the blade metal, the temperature tends to decrease at the trailing edge and increase near the coolant passage. The temperature at the trailing edge is approximately 32 percent below the gas temperature at a thermal conductivity of 120 Btu per hour per foot per °F and 36 percent below the gas temperature at a thermal conductivity of 210 Btu per hour per foot per °F. With increased thermal conductivity, the influence of rim cooling is more effective and the radial distribution lines fall off more rapidly. The temperature differential between the sides and the center of the blade decreases with increased thermal conductivity. For the higher conductivities, this differential is too small to be shown in the figures, inasmuch as it ranges from 2° to 7° F.

An investigation of a rectangular cross-section blade indicates the temperature distribution in a blade having the cross section shown in figure 2 but errors in the temperature distribution will exist. The trend will be indicated, however, if the rectangular cross section is compared with a closer approximation to the true shape; namely, a wedge-shaped section. Figure 9 presents plots of the one-dimensional temperature distribution along the center line at the blade tip for a rectangular and a wedge section at a gas temperature of 2000° F and a thermal conductivity of 15 Btu per hour per foot per °F. The temperature distribution for the wedge shape has a slightly steeper slope than that for the rectangular section and the temperatures at the trailing edge and the wall of the coolant passage are lower. (Part of this lowering is due to the additional thickness of the cooling surface.)

The effect of the thermal conductivity of the blade metal on one-dimensional temperature distribution is shown in figures 10 and 11. Figure 10(a) presents the temperature distribution along the center line of a rectangular section through the outer portion of the blade for an effective gas temperature of 2000° F and various thermal conductivities. At low thermal conductivities, the temperature falls off sharply from the trailing edge to the coolant passage. With increasing thermal conductivity, the temperature decreases at the trailing edge and increases at the wall of the coolant passage, which in general tends to equalize the temperatures across the width of the blade. The reduction of the temperature at the trailing edge increases with an increase in the thermal conductivity. Figure 10(b) shows the temperature distribution for a wedge section for the same conditions imposed on the rectangular section. The general form of the curve is similar to that for the rectangular section; however, the temperatures at the trailing edge and at the wall of the coolant passage are lower and the drop in temperature for a given increase in conductivity is greater.

The variation in temperature with an increase in thermal conductivity for rectangular- and wedge-shaped sections is shown in figure 11. The point selected for comparison was located on the center line of the section at the trailing edge. The curves show that the blade temperature at this point may be considerably lowered by using metals having a high thermal conductivity and that for the same conductivity, the cooling is substantially greater for the more representative wedge-shaped section. This effect is partly due to the loss of effective area at the cooling passage where the thickness of the equivalent rectangular section is considerably less than that of the wedge section. At high values of thermal conductivity a representative temperature distribution can be obtained from the rectangular section by assuming the mean thickness $\bar{t}$ equal to the value of t_2 for the comparative wedge. The total cross-sectional area then is no longer equivalent. The same care in selecting appropriate dimensions extends the useful range of the nondimensional chart (fig. 12).

The nondimensional cooling $\frac{T_e - T}{T_e - T_l}$ at the trailing edge for the rectangle is shown as a function of ab' and q_o/ak in figure 12. Equation (11) was used with $\cosh a\epsilon \approx 1$. It is seen from figure 12 that for $ab' \geq 3$, the cooling is less than 10 percent for the entire range of q_o/ak. In order to obtain 50 percent cooling even for quite large values of q_o/ak, ab' must be less than 1. Points for the extreme values of k, 15 and 210 Btu per hour per foot per $^{\circ}F$, are shown on the figure. Theoretically ab' could be reduced by decreasing q_i and b' or by increasing k and t. Under current conditions, not much can be done about q_i and k. The curves then indicate short thick trailing edges instead of long thin ones for good cooling. From the curves of figure 12 it can be deduced that with materials of low thermal conductivity an infinite increase in the coolant-passage heat-transfer coefficient relative to that obtained with water will have small effect on the trailing-edge temperature.

CONCLUSIONS

The following general conclusions can be drawn from the analysis of the cooling characteristics of the trailing part of a liquid-cooled turbine blade:

1. For blade materials having low thermal conductivity, the computed three-dimensional temperature distribution of the equivalent rectangular trailing section indicates that the rim-cooling effect is significant for only a short distance from the blade root,

the trailing-edge temperature closely approaches the effective gas temperature, and the temperature gradient normal to the surface exposed to the combustion gas can generally be neglected.

2. The three-dimensional and one-dimensional solutions of the equivalent rectangular trailing portion give almost identical temperature distribution in the blade section away from the influence of rim cooling; the one-dimensional treatment of the wedge or rectangular section is therefore sufficient for most investigations.

3. For blade materials of very low thermal conductivity, the one-dimensional temperature distribution computed with the equivalent rectangular section is only slightly different from that of the more representative wedge section.

4. The equations for the one-dimensional rectangular solution permit construction of a simple chart, which gives the value of the trailing-edge nondimensional cooling parameter with any possible combination of the design and operating variables considered in the analysis.

5. For the blade shapes considered in this analysis, and with materials of low thermal conductivity, an infinite increase in the coolant-passage heat-transfer coefficient relative to that obtained with water will have small effect on the trailing-edge temperature.

6. For the blade shapes considered in this analysis, trailing-edge temperature may be considerably reduced with a material of high thermal conductivity and to a lesser extent by locating the cooling passage closer to the trailing edge.

7. Large reduction in trailing-edge temperature results when the blade shape is altered to provide a short thick trailing section.

Aircraft Engine Research Laboratory,
National Advisory Committee for Aeronautics,
Cleveland, Ohio.

APPENDIX A

CALCULATION OF THE INTEGRATION CONSTANTS

The development of equation (34) leads to a determination of N.

$$T_e - T_r = \sum_{1}^{\infty} n \sum_{1}^{\infty} m \left(A_{mn} \cos N_n l' \cosh M_{mn} y' \cos P_m z + B_{mn} \cosh R_{mn} l' \cos \lambda_n y' \cos P_m z\right) \quad (40)$$

The first term will vanish if

$$\cos N_n l' = 0 \quad (41)$$

Thus

$$N_n l' = \left(n - \frac{1}{2}\right)\pi \quad (42)$$

where

$$n = 1, 2, 3, 4, \ldots$$

and

$$N_n = \frac{\left(n - \frac{1}{2}\right)}{l'} \pi \quad (43)$$

For these values of N equation (40) assumes the form

$$T_e - T_r = \sum_{n=1}^{n=\infty} \sum_{m=1}^{m=\infty} B_{mn} \cosh R_{mn} l' \cos \lambda_n y' \cos P_m z \tag{44}$$

Equation (44) is a Fourier development along y' and z.

The development of equation (35) leads to a determination of λ.

$$\sum_{1}^{\infty} m \sum_{1}^{\infty} n \, k(A_{mn} \cos N_n x' \, M_{mn} \sinh M_{mn} b' \cos P_m z - B_{mn} (\cosh R_{mn} x') \lambda_n \sin \lambda_n b' \cos P_m z)$$
$$= \sum_{1}^{\infty} m \sum_{1}^{\infty} n \, q_o (T_e - T_l - A_{mn} \cos N_n x' \cosh M_{mn} b' \cos P_m z - B_{mn} \cosh R_{mn} x' \cos \lambda_n b' \cos P_m z) \tag{45}$$

In order to simplify equation (45) at the boundary condition $y' = b'$ and to solve for the constant λ, the second summation in the left member is equated to the last summation in the right member term by term

Then

$$q_o (T_e - T_l) = \sum_{1}^{\infty} n \sum_{1}^{\infty} m \, A_{mn} (kM_{mn} \sinh M_{mn} b' + q_o \cosh M_{mn} b') \cos P_m z \cos N_n x' \tag{46}$$

and

$$\sum_{1}^{\infty} m \sum_{1}^{\infty} n \, kB_{mn} (\cosh R_{mn} x') \lambda_n \sin \lambda_n b' \cos P_m z = \sum_{1}^{\infty} m \sum_{1}^{\infty} n \, q_o B_{mn} \cosh R_{mn} x' \cos \lambda_n b' \cos P_m z \tag{47}$$

The sums are equated term by term. Therefore, λ_n is determined by any solution of

$$\tan \lambda_n b' = \frac{\frac{q_o b'}{k}}{\lambda_n b'} \tag{48}$$

The development of equation (36) leads to a determination of P.

$$\sum_{1}^{\infty} m \sum_{1}^{\infty} n \; -kA_{mn} \cos N_n x' \cosh M_{mn} y' \left(P_m \sin P_m \frac{t}{2}\right) \; -kB_{mn} \cosh R_{mn} x' \cos \lambda_n y' \left(P_m \sin P_m \frac{t}{2}\right)$$
$$= \sum_{1}^{\infty} m \sum_{1}^{\infty} n \; -q_i \, A_{mn} \cos N_n x' \cosh M_{mn} y' \left(\cos P_m \frac{t}{2}\right) \; -q_i \, B_{mn} \cosh R_{mn} x' \cos \lambda_n y' \left(\cos P_m \frac{t}{2}\right) \tag{49}$$

or

$$\tan P_m \frac{t}{2} = \frac{q_i}{kP_m} = \frac{\frac{q_i t}{2k}}{P_m \frac{t}{2}} \tag{50}$$

The possibility of determining values of B_{mn} and A_{mn} to satisfy equations (44) and (46) has been established in textbooks on Fourier and other harmonic series (reference 6, pp. 118-121), and it is only necessary that the values determined define a convergent series.

The values of A_{mn} are determined by integrating equation (46) between the limits of $x' = 0$ to $x' = l'$ and $z = 0$ to $z = \frac{t}{2}$ and substituting the values previously determined for N_n and P_m in equations (43) and (50). The integration is accomplished in two steps using the function $\cos N_s x dx$ and $\cos P_u z dz$ as multipliers.

For abbreviation,

$$\psi = (kM_{mn} \sinh M_{mn} b' + q_o \cosh M_{mn} b') \tag{51}$$

Then

$$\Psi A_{mn} \cos P_m z \int_{x'=0}^{x'=l'} \cos^2 N_n x' \, dx' = q_o (T_e - T_l) \int_{x'=0}^{x'=l'} \cos N_n x' \, dx' \tag{52}$$

because all the terms

$$\int_o^{l'} \cos N_n x' \cos N_s x' \, dx'$$

vanish when $s \neq n$. When equation (52) is integrated, and the limits substituted

$$\Psi A_{mn} \frac{\cos P_m z}{2N_n} \left[N_n x' + \frac{\sin 2N_n x'}{2} \right]_{x'=0}^{x'=l'} = q_o \left[\frac{(T_e - T_l)}{N_n} \sin N_n x' \right]_{x'=0}^{x'=l'} \tag{53}$$

or

$$\Psi A_{mn} \cos P_m z \left(l' + \frac{\sin 2N_n l'}{2N_n} \right) = 2q_o \frac{(T_e - T_l)}{N_n} \sin N_n l' \tag{54}$$

When the value N_n as determined in equation (43) is substituted

$$\Psi A_{mn} \cos P_m z = \frac{4}{\pi} q_o (T_e - T_l) \frac{(-1)^{n-1}}{2n - 1} = \beta_n \tag{55}$$

When equation (55) is integrated in terms of z using the multiplier $\cos P_u z dz$,

$$\Psi A_{mn} \int_{z=0}^{z=\frac{t}{2}} \cos^2 P_m z dz = \beta_n \int_{z=0}^{z=\frac{t}{2}} \cos P_m z dz \tag{56}$$

because all the terms

$$\int_0^{\frac{t}{2}} \cos P_m z \cos P_u z \, dz$$

vanish when $u \neq m$. The integration of equation (56) gives

$$\psi \frac{A_{mn}}{2P_m} \left[P_m z + \frac{\sin 2P_m z}{2} \right]_{z=0}^{z=\frac{t}{2}} = \frac{\beta_n}{P_m} \left[\sin P_m z \right]_0^{\frac{t}{2}} \tag{57}$$

Substituting limits,

$$\psi A_{mn} \left(\frac{t}{2} + \frac{\sin 2P_m \frac{t}{2}}{2P_m} \right) = \frac{2\beta_n \sin P_m \frac{t}{2}}{P_m} \tag{58}$$

or

$$A_{mn} = 2 \frac{\beta_n}{P_m \frac{t}{2}} \frac{\sin P_m \frac{t}{2}}{\left(1 + \frac{\sin 2P_m \frac{t}{2}}{2P_m \frac{t}{2}} \right)} \frac{1}{\psi} \tag{59}$$

In like manner B_{mn} is determined from equation (44) and the equation for B_{mn} is

$$B_{mn} = 2\zeta_n \frac{\sin P_m \frac{t}{2}}{P_m \frac{t}{2}} \frac{1}{\cosh R_{mn} l' \left(1 + \frac{\sin 2P_m \frac{t}{2}}{2P_m \frac{t}{2}} \right)} \tag{60}$$

where

$$\zeta_n = 2\,(T_e - T_r)\,\frac{\sin \lambda_n b'}{\lambda_n b'}\,\frac{1}{\left(1 + \frac{\sin 2\lambda_n b'}{2\lambda_n b'}\right)} \tag{61}$$

APPENDIX B

EVALUATION OF THE TERMS WHERE m > 1

The temperature distribution in the turbine blade under consideration is determined neglecting the smaller terms when $m > 1$ and using equation (37) in the form

$$\theta = \cos P_1 z \sum_{1}^{\infty} n \left(A_{1n} \cos N_n x' \cosh M_{1n} y' + B_{1n} \cosh R_{1n} x' \cos \lambda_n y'\right) \tag{62}$$

This equation will be valid for all practical purposes when the thickness of the blade is small compared with the width and the length. It is necessary, in demonstrating this statement, to expand the double series given by equation (37) and inspect the terms containing the function $\cos P_m z$. The expansion of equation (37) with the subscripts in the order mn assumes the form

$$\begin{aligned}
\theta = {} & (A_{11} \cosh M_{11} y' \cos P_1 z + A_{21} \cosh M_{21} y' \cos P_2 z + \ldots) \cos N_1 x' \\
& + (A_{12} \cosh M_{12} y' \cos P_1 z + A_{22} \cosh M_{22} y' \cos P_2 z + \ldots) \cos N_2 x' \\
& + \ldots + (A_{1n} \cosh M_{1n} y' \cos P_1 z + A_{2n} \cosh M_{2n} y' \cos P_2 z + \ldots) \cos N_n x' \\
& + (B_{11} \cosh R_{11} x' \cos P_1 z + B_{21} \cosh R_{21} x' \cos P_2 z + \ldots) \cos \lambda_1 y' \\
& + (B_{12} \cosh R_{12} x' \cos P_1 z + B_{22} \cosh R_{22} x' \cos P_2 z + \ldots) \cos \lambda_2 y' \\
& + \ldots + (B_{1n} \cosh R_{1n} x' \cos P_1 z + B_{2n} \cosh R_{2n} x' \cos P_n z + \ldots) \cos \lambda_n y'
\end{aligned} \tag{63}$$

If all the other terms in the series are arranged so they become coefficients of the function $\cos P_m z$,

$$\theta = A_{11} \cosh M_{11}y' \left(\cos P_1 z + \frac{A_{21} \cosh M_{21}y'}{A_{11} \cosh M_{11}y'} \cos P_2 z + \ldots\right) \cos N_1 x'$$

$$+ A_{12} \cosh M_{12}y' \left(\cos P_1 z + \frac{A_{22} \cosh M_{22}y'}{A_{12} \cosh M_{12}y'} \cos P_2 z + \ldots\right) \cos N_2 x' + \ldots$$

$$+ A_{1n} \cosh M_{1n}y' \left(\cos P_1 z + \frac{A_{2n} \cosh M_{2n}y'}{A_{1n} \cosh M_{1n}y'} \cos P_2 z + \ldots\right) \cos N_n x'$$

$$+ B_{11} \cosh R_{11}x' \left(\cos P_1 z + \frac{B_{21} \cosh R_{21}x'}{B_{11} \cosh R_{11}x'} \cos P_2 z + \ldots\right) \cos \lambda_1 y'$$

$$+ B_{12} \cosh R_{12}x' \left(\cos P_1 z + \frac{B_{22} \cosh R_{22}x'}{B_{12} \cosh R_{12}x'} \cos P_2 z + \ldots\right) \cos \lambda_2 y'$$

$$+ B_{1n} \cosh R_{1n}x' \left(\cos P_1 z + \frac{B_{2n} \cosh R_{2n}x'}{B_{1n} \cosh R_{1n}x'} \cos P_2 z + \ldots\right) \cos \lambda_n y' \qquad (64)$$

From equation (64) it can be seen that if the coefficient of the function $\cos P_2 z$ in any series is negligible compared with unity, the terms subsequent to $\cos P_1 z$ may be disregarded for practical application of the equation. Because the series is convergent for ascending values of n, it is only necessary to inspect the coefficient of $\cos P_2 z$ for a value of $n = 1$.

When the coefficient of $\cos P_2 z$ in the A_{mn} series is equated to ϕ and the values of A_{mn} determined by equation (59) are substituted,

$$\phi = \frac{\dfrac{\sin P_2 \frac{t}{2}}{P_2 \frac{t}{2}}}{\dfrac{\sin P_1 \frac{t}{2}}{P_1 \frac{t}{2}}} \frac{\left(1 + \dfrac{\sin 2P_1 \frac{t}{2}}{2P_1 \frac{t}{2}}\right)}{\left(1 + \dfrac{\sin 2P_2 \frac{t}{2}}{2P_2 \frac{t}{2}}\right)} \frac{(kM_{11} \sinh M_{11}b' + q_o \cosh M_{11}b') \cosh M_{21}y'}{(kM_{21} \sinh M_{21}b' + q_o \cosh M_{21}b') \cosh M_{11}y'} \qquad (65)$$

or

$$\phi = \frac{\dfrac{\sin P_2 \frac{t}{2}}{P_2 \frac{t}{2}}\left(1+\dfrac{\sin 2P_1 \frac{t}{2}}{2P_1 \frac{t}{2}}\right)}{\dfrac{\sin P_1 \frac{t}{2}}{P_1 \frac{t}{2}}\left(1+\dfrac{\sin 2P_2 \frac{t}{2}}{2P_2 \frac{t}{2}}\right)} \frac{(kM_{11} \tanh M_{11}b' + q_o)}{(kM_{21} \tanh M_{21}b' + q_o)} \frac{\cosh M_{11}b'}{\cosh M_{21}b'} \frac{\cosh M_{21}y'}{\cosh M_{11}y'} \quad (66)$$

For the blade under consideration,

$b' = 0.055$ ft

$k = 15$ Btu/(hr)(ft)($^\circ$F)

$l' = 0.3383$ ft

$q_i = 222$ Btu/(hr)(sq ft)($^\circ$F)

$q_o = 2370$ Btu/(hr)(sq ft)($^\circ$F)

$t = 0.01$ ft

From equation (50)

$P_1 = 53.74$

$P_2 = 632.99$

From equation (43)

$N_1 = 4.64$ ft^{-1}

From equation (38)

$M_{11} = 53.94$ ft^{-1}

$M_{21} = 632.99$ ft^{-1}

The following circular and hyperbolic functions apply for these values:

$\sin P_1 \frac{t}{2} = 0.2654$ $\quad \cosh M_{11}b' = 9.7425$

$\sin P_2 \frac{t}{2} = .0234$ $\quad \cosh M_{21}b' = 6.5907 \times 10^{14}$

$\sin 2P_1 \frac{t}{2} = 0.5119$ $\quad \cosh M_{11}y' = 1$ when $y' = 0$

$\sin 2P_2 \frac{t}{2} = .0467$ $\quad \cosh M_{21}y' = 1$ when $y' = 0$

$\tanh M_{11}b' = 0.995$ $\quad \cosh M_{11}y' = 7.4513$ when $y' = .05$

$\tanh M_{21}b' = 1$ $\quad \cosh M_{21}y' = 2.7822 \times 10^{13}$ when $y' = .05$

If the given values in equation (66) are substituted, the following coefficients are obtained:

$y' = 0$	$\phi = -5.738 \times 10^{-17}$
$y' = 0.05$	$\phi = -2.142 \times 10^{-4}$
$y' = b'$	$\phi = -3.882 \times 10^{-3}$

The values of ϕ obtained for the blade under consideration show that the coefficient of the $\cos P_2 z$ term has a maximum value at $y' = b'$ and is then equal to 0.4 percent of the first term and as such may be disregarded for practical applications.

The effect of the second term of the B_{mn} series can be investigated by equating the coefficient of the $\cos P_2 z$ term to x and the previous process repeated.

$$\Gamma = \frac{\dfrac{\sin P_2 \frac{t}{2}}{P_2 \frac{t}{2}}}{\dfrac{\sin P_1 \frac{t}{2}}{P_1 \frac{t}{2}}} \frac{\left(1 + \dfrac{\sin 2P_1 \frac{t}{2}}{2P_1 \frac{t}{2}}\right)}{\left(1 + \dfrac{\sin 2P_2 \frac{t}{2}}{2P_2 \frac{t}{2}}\right)} \frac{\cosh R_{11} l'}{\cosh R_{21} l'} \frac{\cosh R_{21} x'}{\cosh R_{11} x'} \qquad (67)$$

The application of equation (67) to the blade under consideration requires the following values:

From equation (48)

$$\lambda_1 = 25.64 \text{ ft}^{-1}$$

From equation (39)

$$R_{11} = 59.54 \text{ ft}^{-1}$$

$$R_{21} = 633.51 \text{ ft}^{-1}$$

With the values of R_{mn} and l' used, the $\cosh R_{mn}l'$ and $\cosh R_{mn}x'$ may be approximated by $\frac{e^{R_{mn}l'}}{2}$ and equation (67) becomes

$$\Gamma = \frac{\frac{\sin P_2 \frac{t}{2}}{P_2 \frac{t}{2}}\left(1 + \frac{\sin 2P_1 \frac{t}{2}}{2P_1 \frac{t}{2}}\right)}{\frac{\sin P_1 \frac{t}{2}}{P_1 \frac{t}{2}}\left(1 + \frac{\sin 2P_2 \frac{t}{2}}{2P_2 \frac{t}{2}}\right)} e^{(l'-x')(R_{11}-R_{21})} \qquad (68)$$

When the given values in equation (68) are substituted for a range of values of x', the following values of Γ are found:

x' (ft)	Distance from rim (ft)	Γ
0.005	0.3333	
.3283	.01	-0.4643×10^{-4}
.3333	.005	$- .8227 \times 10^{-3}$
.3383	0	$- .1451 \times 10^{-1}$

The coefficient of the $\cos P_m z$ term increases as the rim is approached and reaches a value of 1.5 percent of the first term at this point. For purposes of this report, the temperature will not be calculated within 0.005 foot of the rim and the cooling liquid. With this limitation, the values of the second and subsequent terms are negligible.

REFERENCES

1. Brown, W. Byron: Cooling of Gas Turbines. I - Effect of Addition of Fins to Blade Tips and Rotor, Admission of Cooling Air through Part of Nozzles, and Change in Thermal Conductivity of Turbine Components. NACA RM No. E7B11a, 1947.

2. Wolfenstein, Lincoln, Meyer, Gene L., and McCarthy, John S.: Cooling of Gas Turbines. II - Effectiveness of Rim Cooling of Blades. NACA RM No. E7B11b, 1947.

3. Brown, W. Byron, and Livingood, John N. B.: Cooling of Gas Turbines. III - Analysis of Rotor and Blade Temperatures for Liquid-Cooled Gas Turbines. NACA RM No. E7B11c, 1947.

4. Harper, D. R., 3d, and Brown, W. B.: Mathematical Equations for Heat Conduction in the Fins of Air-Cooled Engines. NACA Rep. No. 158, 1922.

5. McAdams, William H.: Heat Transmission. McGraw-Hill Book Co., Inc., 2d ed., 1942, p. 168.

6. Byerly, William Elwood: An Elementary Treatise on Fouriers Series and Spherical, Cylindrical, and Ellipsoidal Harmonics. Ginn and Co., 1893.

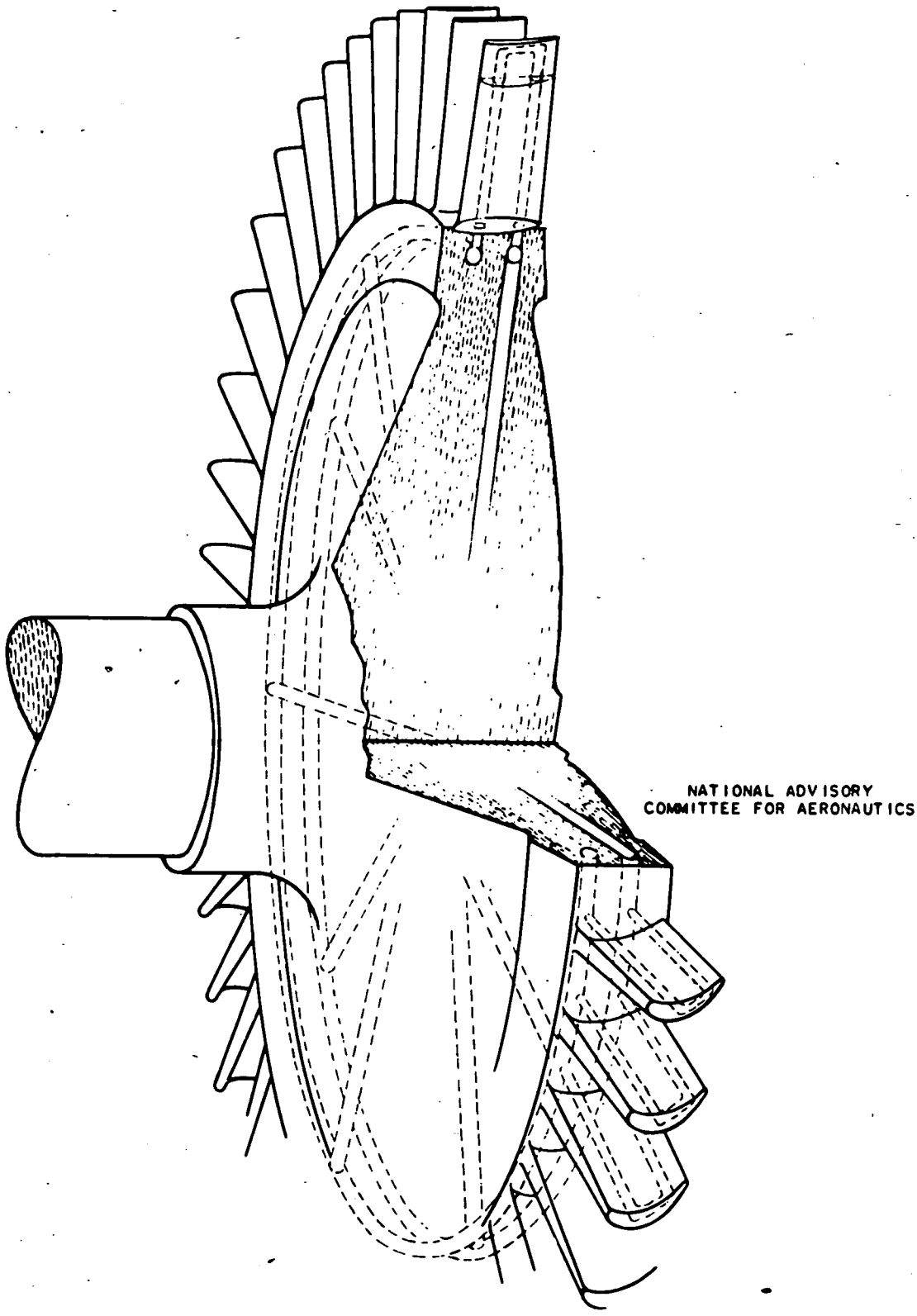

Figure 1. - Arrangement of internal-cooling passages.

Figure 2. - Blade section showing cooling passages.

NATIONAL ADVISORY
COMMITTEE FOR AERONAUTICS

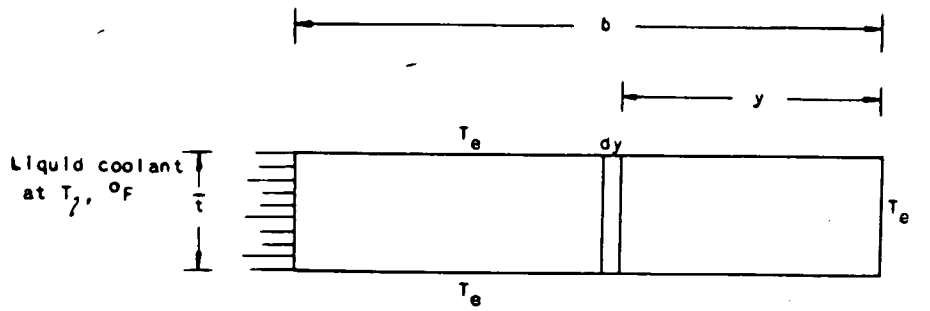

Figure 3. - Rectangular approximation to rear part of blade section for one-dimensional analysis.

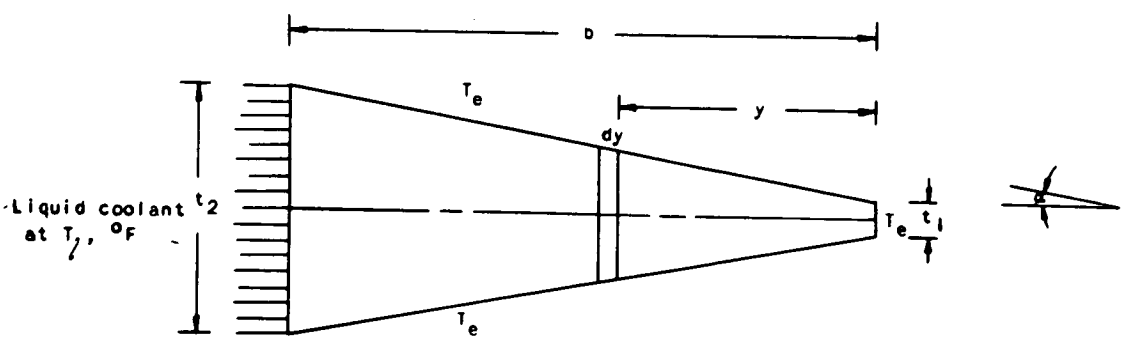

Figure 4. - Wedge-shaped approximation to rear part of blade sections for one-dimensional analysis.

NATIONAL ADVISORY
COMMITTEE FOR AERONAUTICS

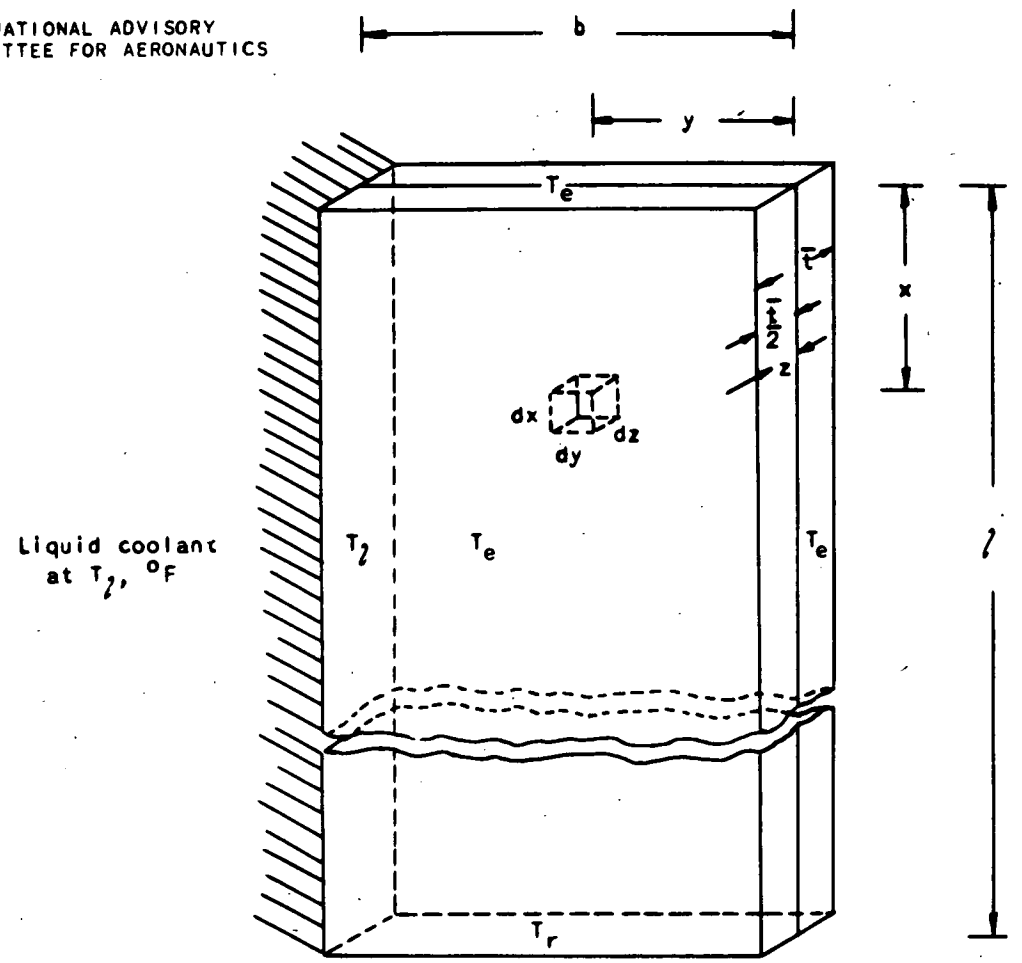

Figure 5. - Rectangular approximation to rear part of 4-inch-turbine blade for three-dimensional analysis.

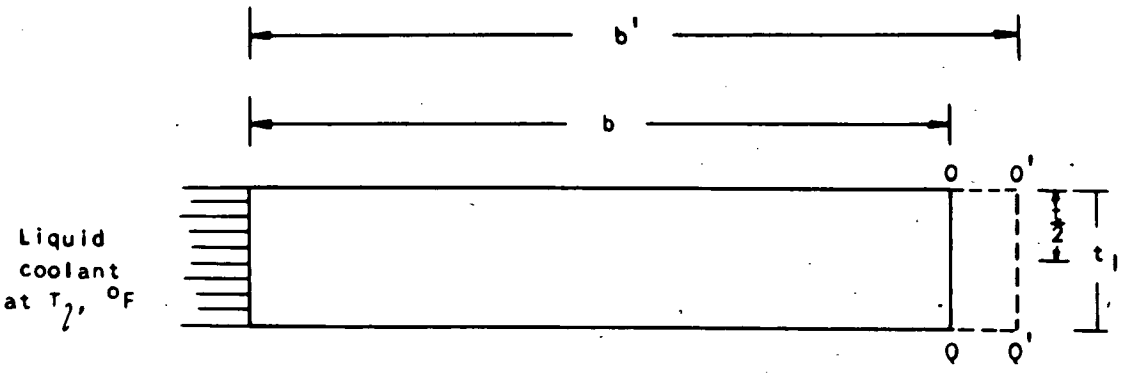

Figure 6. - Correction for heat received by trailing edge.

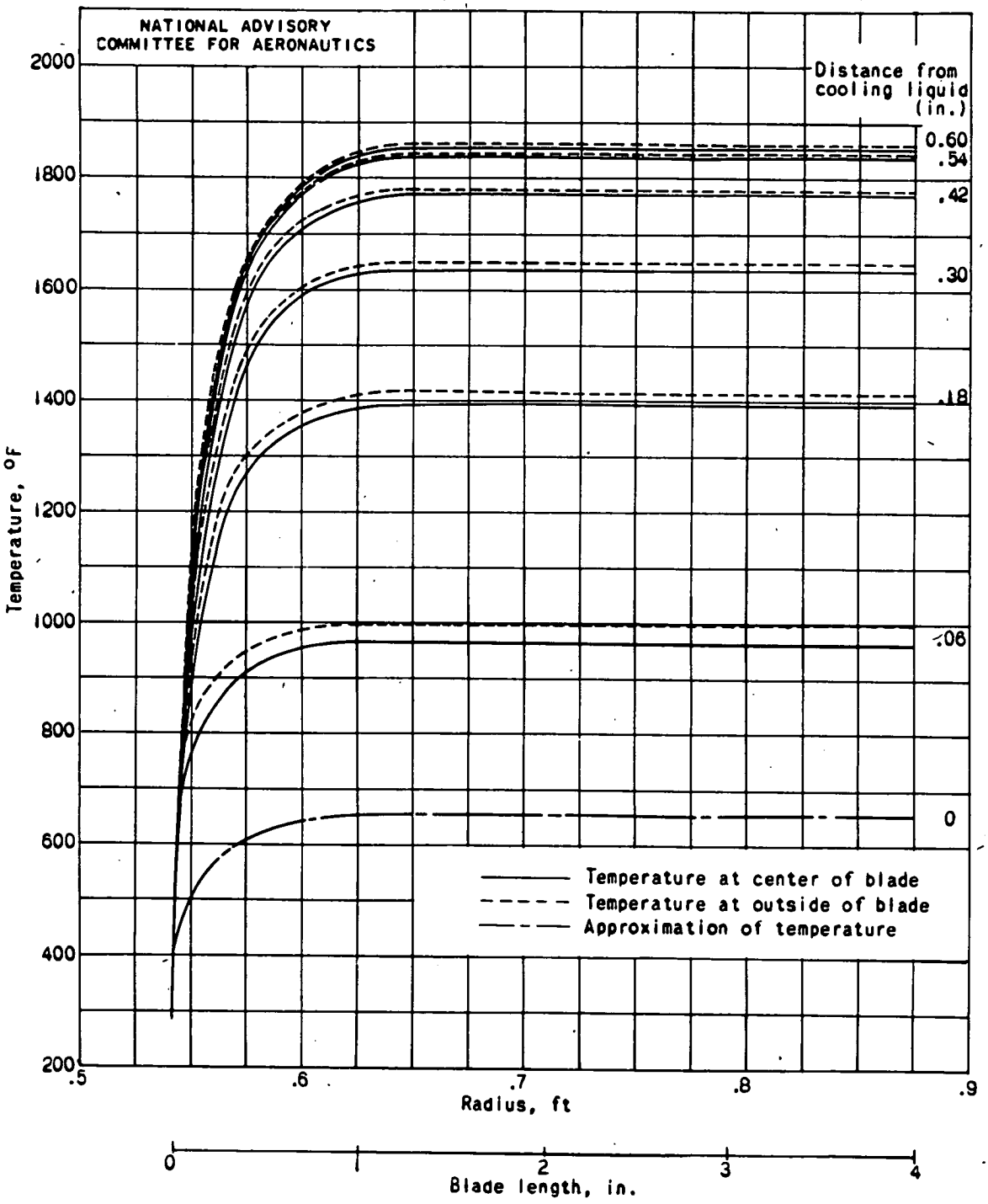

(a) Effective gas temperature, T_e, 2000° F.

Figure 7. - Three-dimensional temperature distribution in rear part of turbine blade at thermal conductivity k of 15 Btu/(hr)(ft)(°F). (For facility in reading, fig. 7 (a) is plotted on a different ordinate scale than figs. 7(b) and (c).)

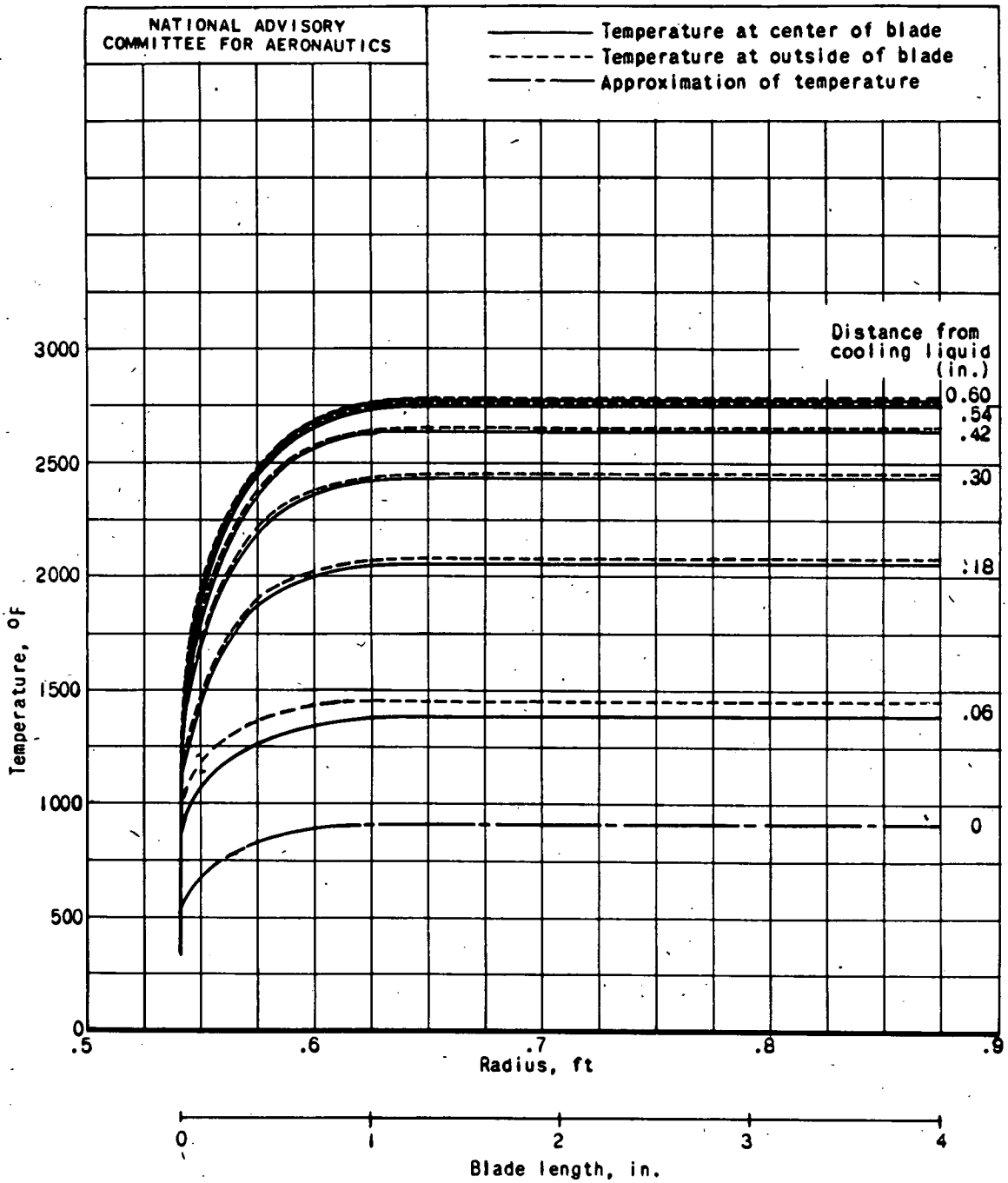

(b) Effective gas temperature, T_e, 3000° F.

Figure 7. - Continued. Three-dimensional temperature distribution in rear part of turbine blade at thermal conductivity k of 15 Btu/(hr)(ft)(°F).

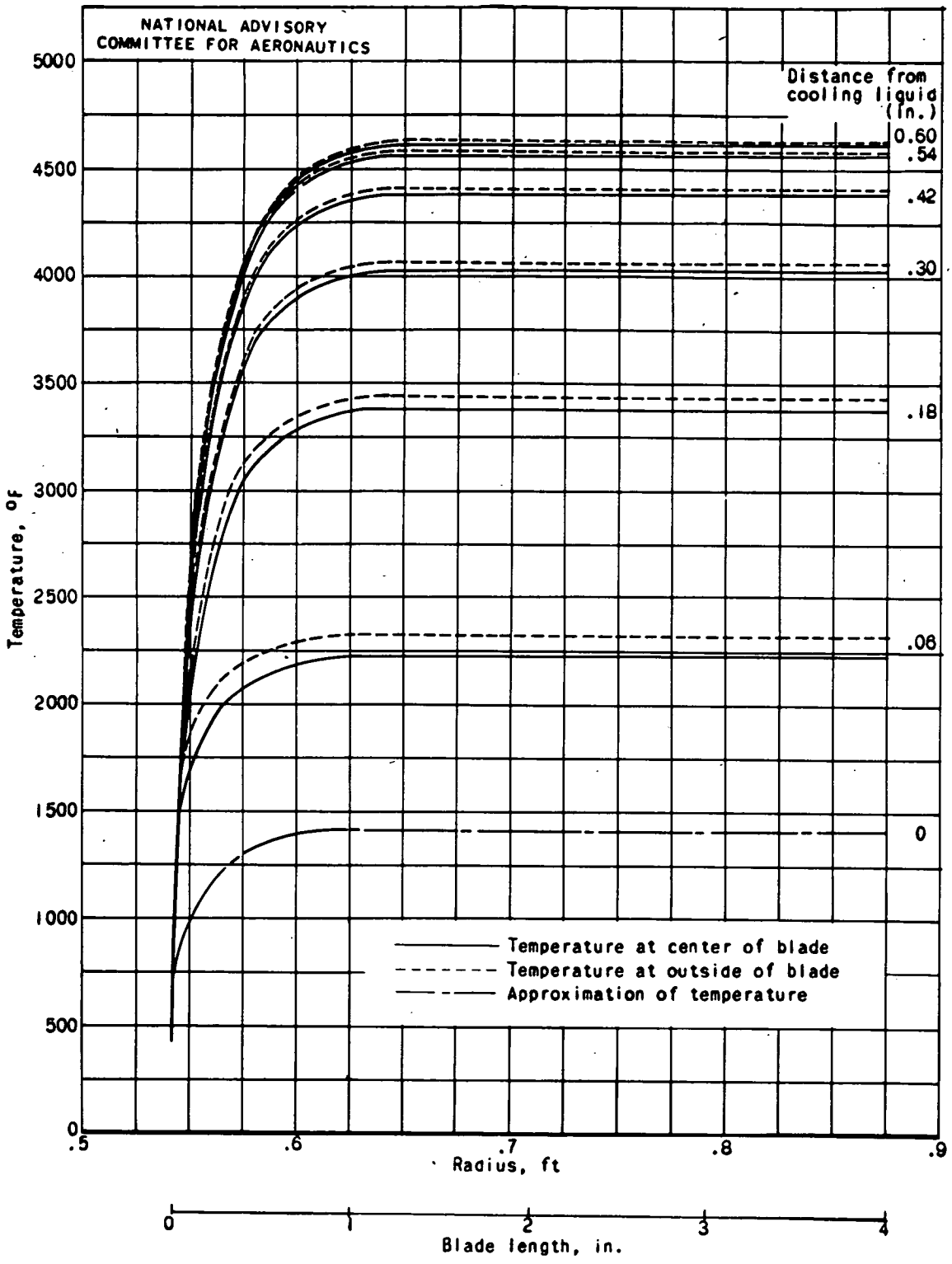

(c) Effective gas temperature, T_e, 5000° F.

Figure 7. - Concluded. Three-dimensional temperature distribution in rear part of turbine blade at thermal conductivity k of 15 Btu/(hr)(ft)(°F).

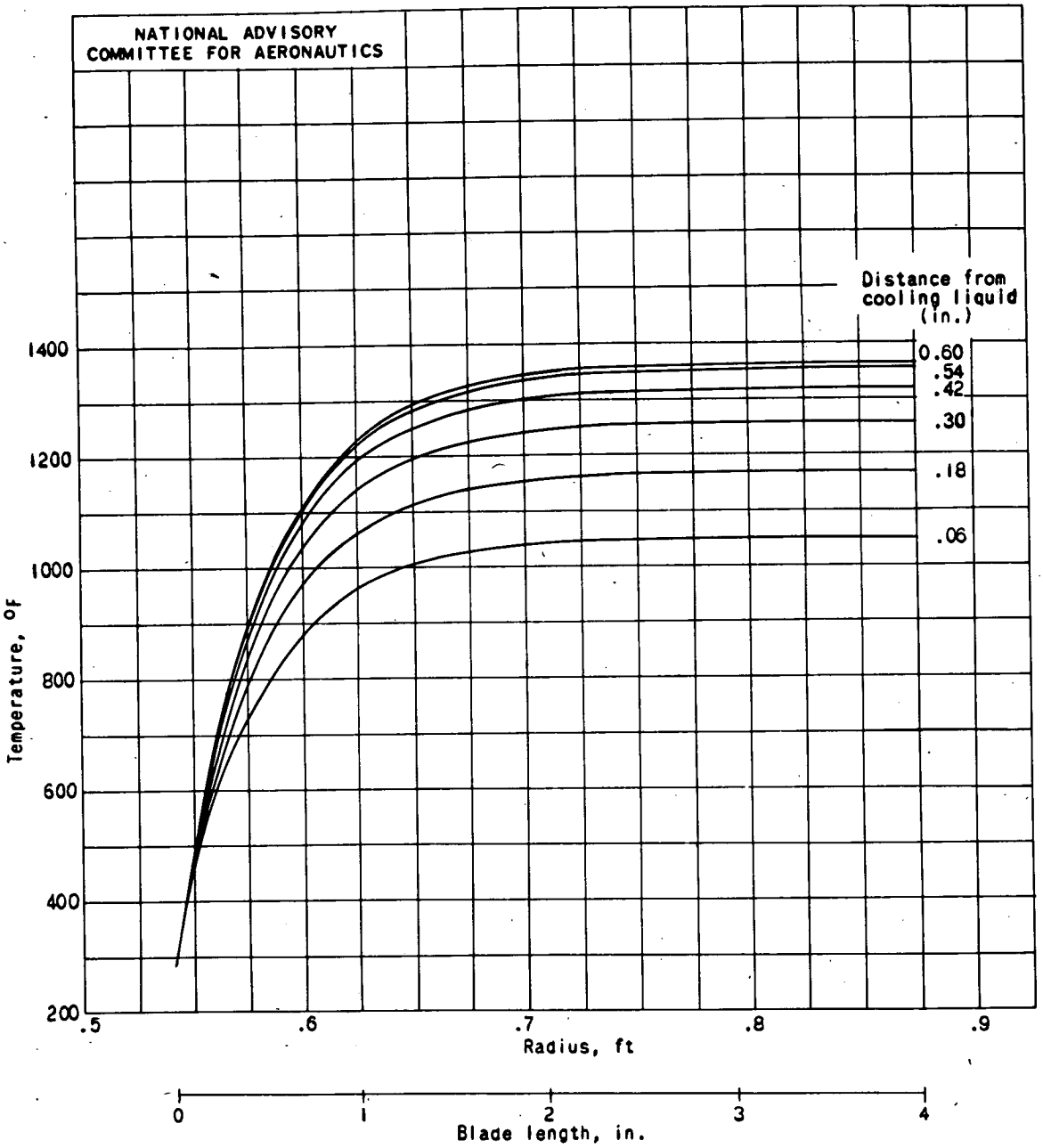

(a) Thermal conductivity, k, 120 Btu/(hr)(ft)(°F).

Figure 8. - Three-dimensional temperature distribution in rear part of turbine blade at effective gas temperature T_e of 2000° F.

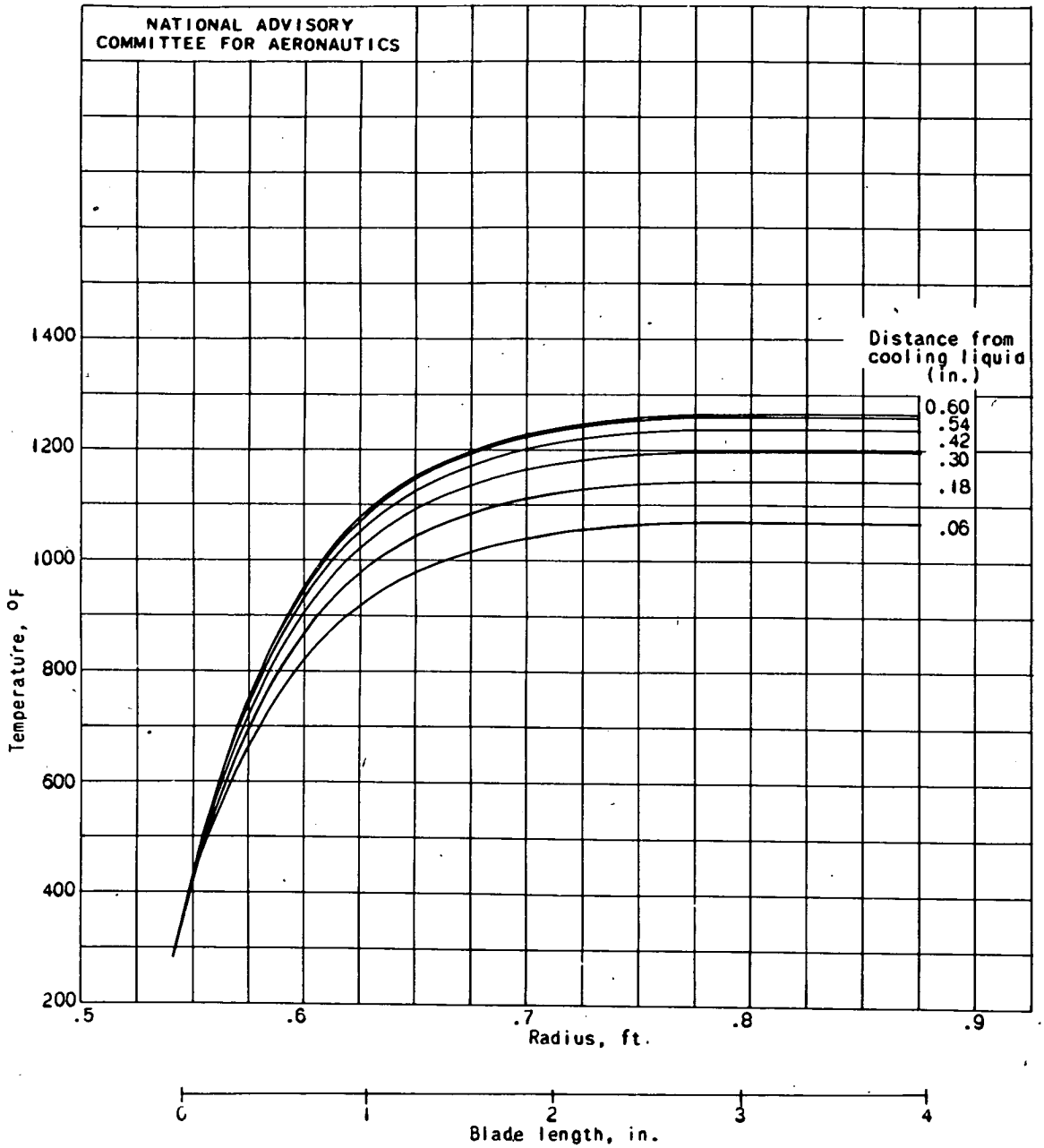

(b) Thermal conductivity, K, 210 Btu/(hr)(ft)(°F).

Figure 8. - Concluded. Three-dimensional temperature distribution in rear part of turbine blade at effective gas temperature T_e of 2000° F.

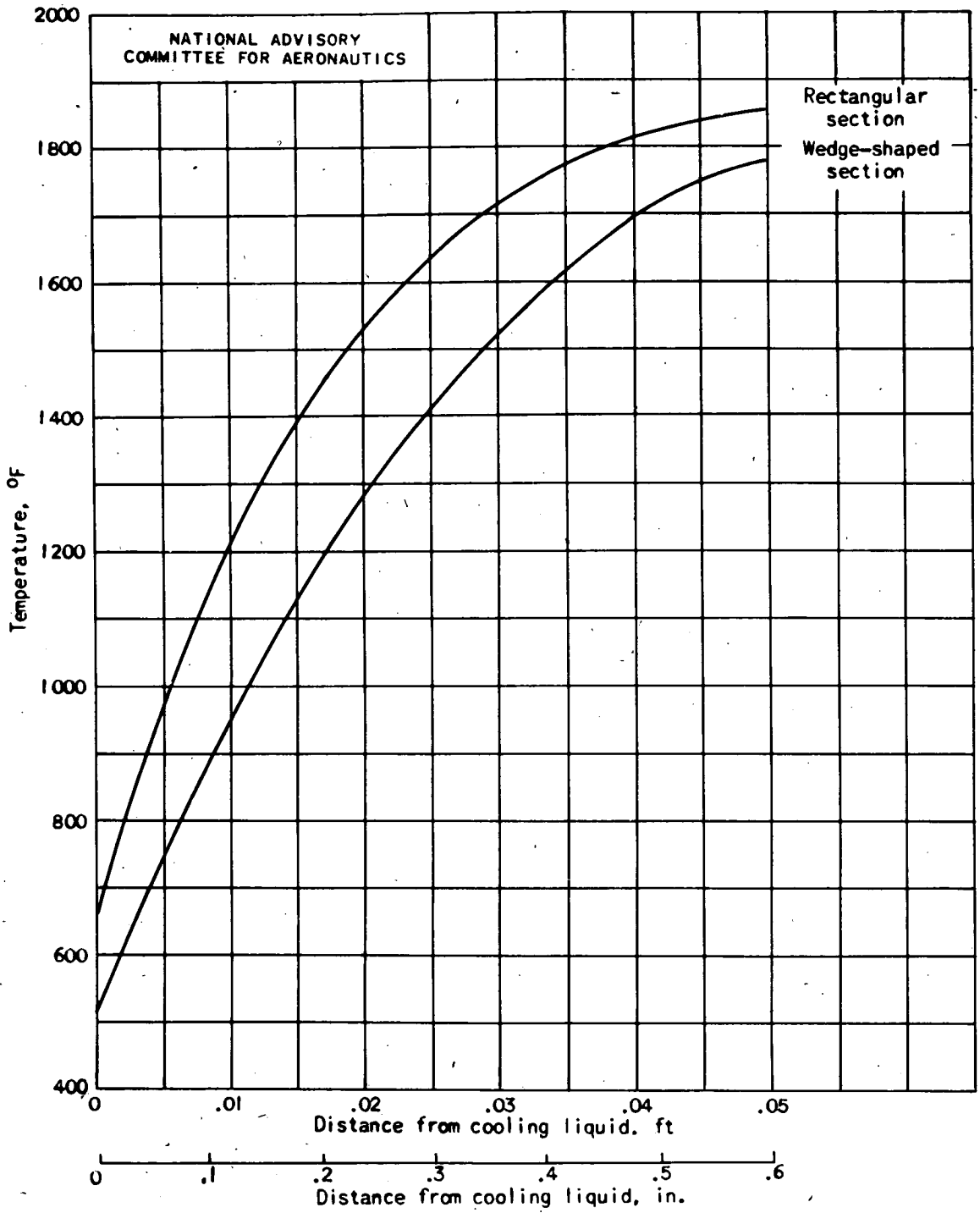

Figure 9. - One-dimensional analysis of the effect of shape on prevelanet blade temperature. Effective gas temperature, T_e, 2000° F; thermal conductivity k, 15 Btu/(hr)(ft)(°F).

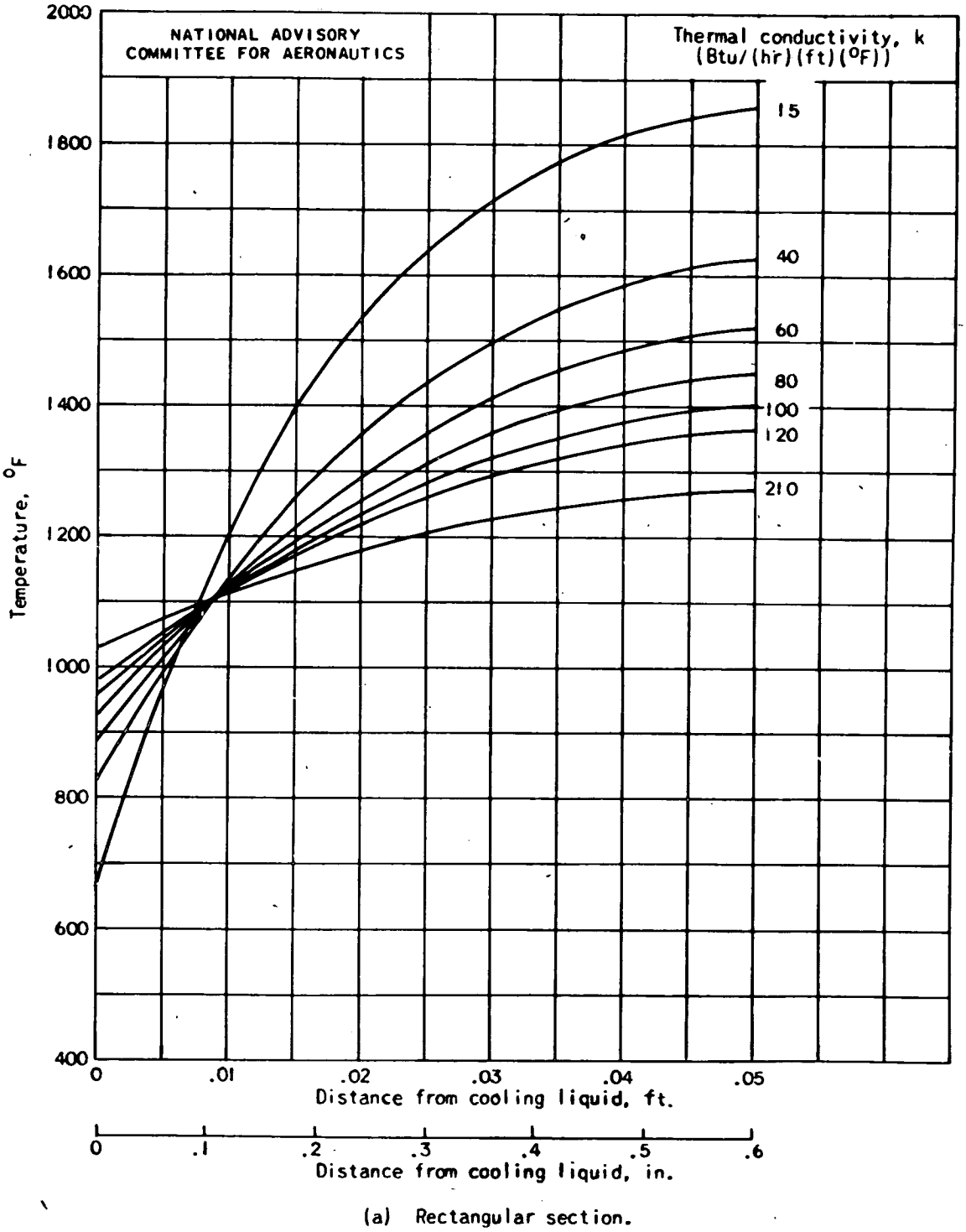

(a) Rectangular section.

Figure 10. - One-dimensional solution for pervalent blade temperature at effective gas temperature T_e of 2000° F.

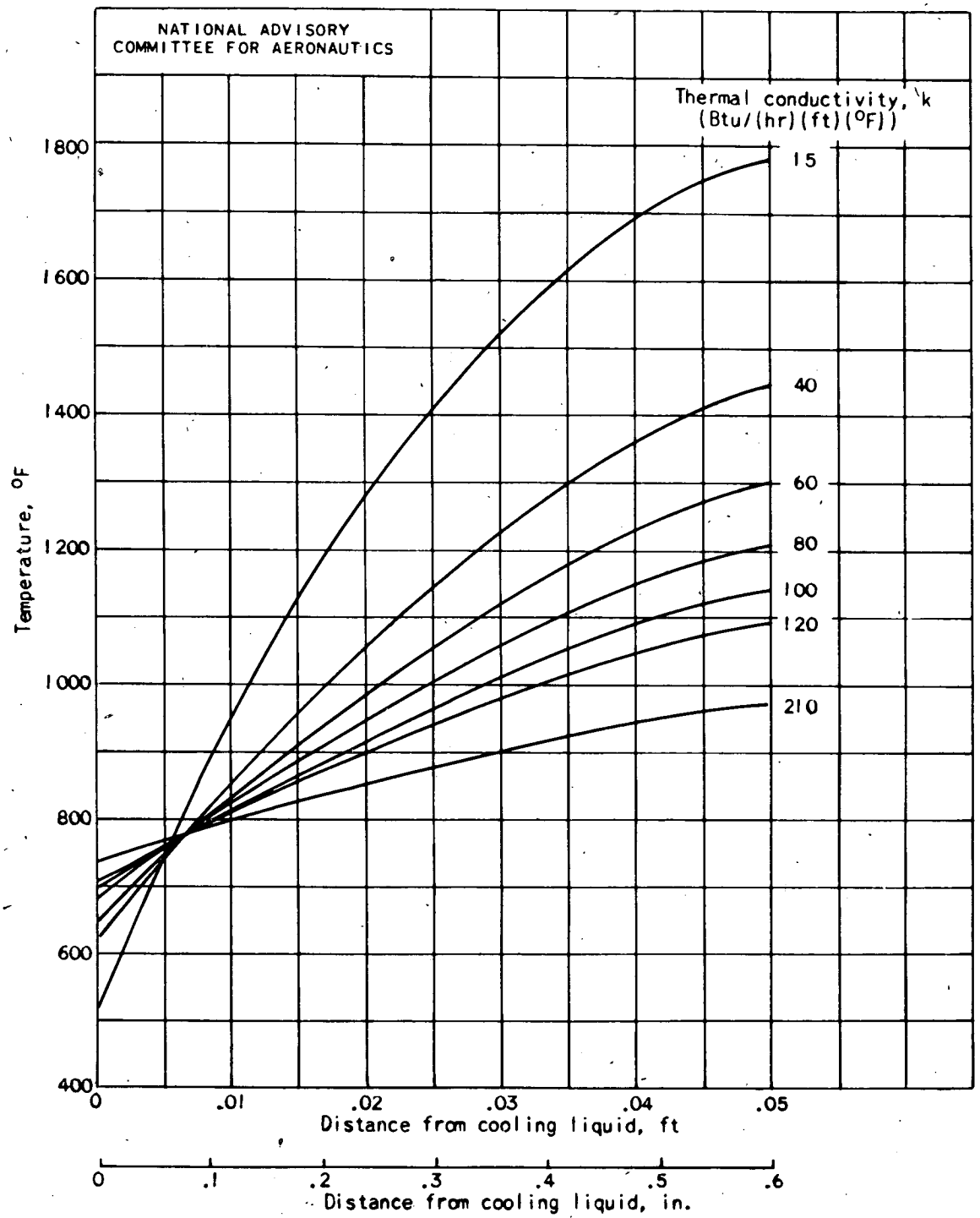

(b) Wedge-shaped section.

Figure 10. - Concluded. One-dimensional solution for prevalent blade temperature at effective gas temperature T_e of 2000° F.

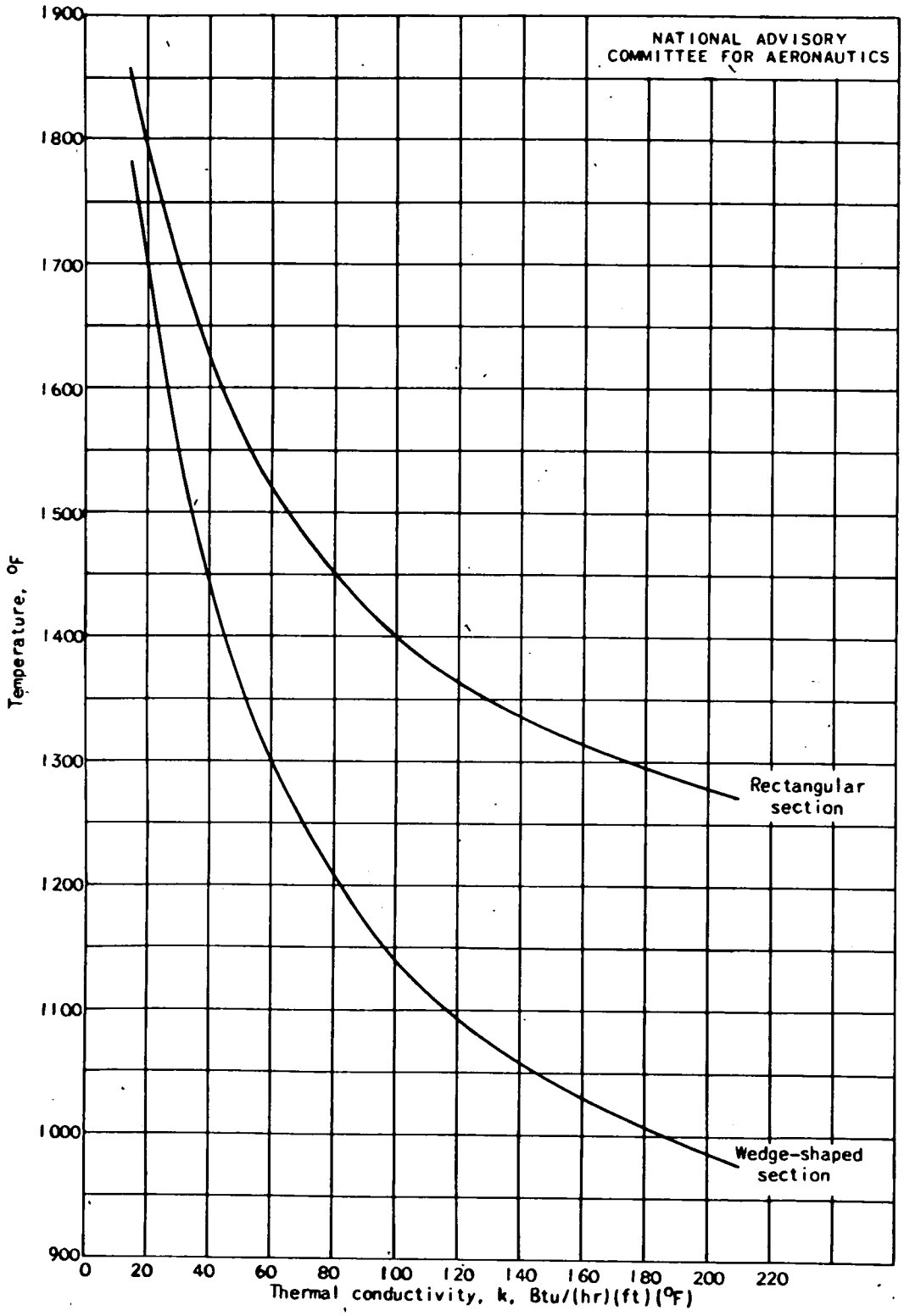

Figure 11. – Temperatures of trailing edge obtained from the one-dimensional solutions. Effective gas temperature, T_e, 2000° F.

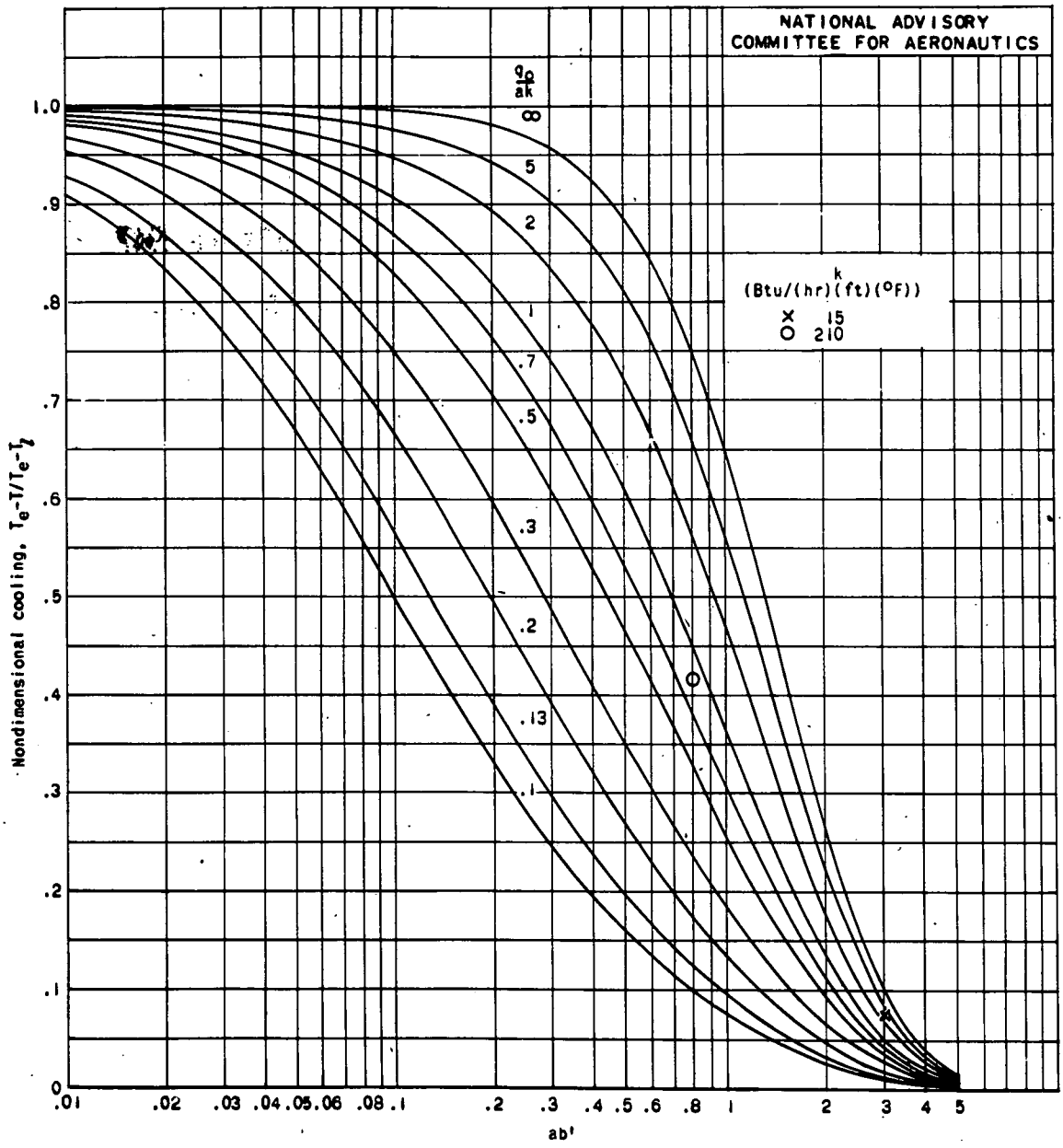

Figure 12. - Nondimensional cooling at the trailing edge T_e-T/T_e-T_i as a function of dimensionless parameters ab' and q_o/ak when $a = \sqrt{2q_i/kt}$.